We are IntechOpen, the world's leading publisher of Open Access books Built by scientists, for scientists

6,900
Open access books available

185,000
International authors and editors

200M
Downloads

Our authors are among the

154
Countries delivered to

TOP 1%
most cited scientists

12.2%
Contributors from top 500 universities

WEB OF SCIENCE™

Selection of our books indexed in the Book Citation Index in Web of Science™ Core Collection (BKCI)

Interested in publishing with us?
Contact book.department@intechopen.com

Numbers displayed above are based on latest data collected.
For more information visit www.intechopen.com

Chapter 3

Computational Fluid Dynamics Method for the Analysis of the Hydrodynamic Performance in Swimming

Ahlem Arfaoui and Guillaume Polidori

Additional information is available at the end of the chapter

http://dx.doi.org/10.5772/61176

Abstract

Numerical simulations of the flow around a swimmer during the different swimming phases were carried out to understand the drag force. In mechanics of swimming, the reduction of forces, which oppose to the swimmers advancement, plays a very important part in the improvement of the performances. As a consequence, the performance improvement requires a better understanding of the structure of the fluid flow around swimmers and a good knowledge of the pressure fields and wall shear stress encountered to minimize them. This chapter will focus on computational fluid dynamics (CFD) procedures and results for this practical implication in swimming and will aim at highlighting details on numerical schemes, validations, and results showing the way CFD can be used as a powerful tool in swimming understanding.

Keywords: CFD, swimming, standard kk–$\omega\omega$ turbulence model, underwater surface patterns, head positions

1. Introduction

In the mechanics of swimming, the study of the flow features around the swimmer during the different swimming phases is of great importance. The hydrodynamic performance in swimming depends strongly on the technique adopted by the swimmers during the different phases of swimming as well as on the resistance of advancement encountered during their movements in water. Three drag forces are noted when the swimmer advances in water, namely, friction drag due to the viscosity of water, pressure drag due to the complex shape of the human body, and wave drag created at the surface of the water. The performance improvement requires a better understanding of the structure of the fluid flow around swimmers and a good knowledge of the pressure fields and wall shear stress encountered to minimize them.

INTECH
open science | open minds

© 2015 The Author(s). Licensee InTech. This chapter is distributed under the terms of the Creative Commons Attribution License (http://creativecommons.org/licenses/by/3.0), which permits unrestricted use, distribution, and reproduction in any medium, provided the original work is properly cited.

In literature, research in swimming was poor until 1970. Some authors measured the total drag on the swimmer's whole body and estimated the influence of various parameters such as the morphology of swimmer, the position of swimmer, or the velocity on the level of the drag and on analysis of performance. In the quest for higher levels of performance in swimming, many research strategies have been adopted to reduce drag to optimize and coordinate the different movements. Due to the complexity in the use of different experimental measurement techniques, researchers are oriented toward the numerical simulation using computational fluid dynamics (CFD) method. The CFD method is increasingly used in the domain of biomechanics notably to study the flow around a different parts of swimmer's body.

In swimming, the first study that used the CFD method on a real model is that of Bixler and Riewald [1]. They have used CFD to approach the flow around the hand and forearm of a swimmer. The numerical modeling was to calculate the forces and hydrodynamic coefficients for different angles of attack. In same time, the flow around the hand and forearm was also studied by Sato and Hino [2] using the CFD. The purpose of their work was to establish a method to predict the thrust force and optimize the movement of the swimmer while swimming.

In 2006, Rouboa et al. [3] used CFD in order to calculate the drag and lift coefficients for the hand and forearm of a swimmer in steady and unsteady cases, as well as to assess the effect of accelerating the hand and forearm on generating the propulsion force. The model of the hand and forearm used in the numerical simulation was built using a CAD (Computer Aided Design) based on the dimensions of a model of the hand and forearm of a male subject. Since then, the CFD method has been used by several authors in the swimming field.

This chapter will focus on CFD procedures and results for this practical implication in swimming and will aim at highlighting details on numerical schemes, validations, and results showing the way CFD can be used as a powerful tool in swimming understanding.

2. Mathematical modeling

When an elongated element is studied such as a swimmer for example, the flow around this element becomes unstable and turbulent. This instability occurs when Re is about 5×10^5 for streamlined bodies. Therefore, the turbulent fluid flow is controlled by the Reynolds averaged Navier–Stokes equations. These equations are obtained by decomposing each instantaneous variable (velocity, pressure, etc.) into a mean component and a fluctuating component, and by time averaging the instantaneous governing equations. This method is based on the spatial integration of the conservation equations over finite control volumes.

The way to choose the turbulence model is of great importance to highlight vortex structures and recirculation zones in the vicinity of the swimmer's body.

2.1. Governing equations

In fluid mechanics, one of the fundamental parameters used when a fluid is in relative motion to a surface is the Reynolds number (Re), including the fluid properties of density and viscosity, plus a velocity and a characteristic dimension:

http://dx.doi.org/10.5772/61176

$$R_e = \frac{inertialforces}{viscousforces} = \frac{\rho \mathbf{v} L}{\mu} = \frac{\mathbf{v} L}{\nu}$$

where **v** is the mean velocity of the object relative to the fluid (SI units: m/s), L is a characteristic linear dimension (m), and ν is the kinematic viscosity (m²/s).

The resulting system of equations to be solved for this two-dimensional incompressible flow in steady-state regime is as follows:

Continuity equation:

$$\frac{\partial}{\partial x_i}(\overline{U_i}) = 0 \tag{1}$$

Navier–Stokes (momentum) equations:

$$\frac{\partial}{\partial x_j}(\rho \bar{U}_i \bar{U}_j) = -\frac{\partial \bar{p}}{\partial x_i} + \frac{\partial}{\partial x_j}\left[\mu\left(\frac{\partial \bar{U}_i}{\partial x_j} + \frac{\partial \bar{U}_j}{\partial x_i}\right) - \rho\overline{u_i u_j}\right] \tag{2}$$

Boussinesq hypothesis:

$$-\rho\overline{u_i u_j} = \mu_t\left(\frac{\partial \bar{U}_i}{\partial x_j} + \frac{\partial \overline{U_j}}{\partial x_i}\right) - \frac{2}{3}\delta_{ij}\rho k \tag{3}$$

where $U_i(t) \equiv U_i = \overline{U_i} + u_i$: instantaneous velocity component in the i direction (m/s); $\overline{\boldsymbol{U}}_{\boldsymbol{i}}$: mean (time-averaged) velocity component in the i direction (m/s); u_i: fluctuating velocity component in the i direction (m/s); i, j: directions; μ_t: turbulent viscosity (kg/ms); and ρ: fluid density (kg/m^3)

A new term, $-\rho\overline{u_i u_j}$, due to the correlation between the fluctuations of the velocity components appears in the time-averaged governing equations. This term, also called Reynolds stresses, is problematic as the number of unknowns becomes greater than the number of equations. The aim of the various turbulence models proposed in the literature is to model the Reynolds stresses in order to close the system of equations to be solved. The Boussinesq hypothesis can be used to approach the Reynolds stresses [4]. This hypothesis consists in directly linking the correlations with the time-averaged velocity components by the introduction of the concept of turbulent viscosity (μ_t). The turbulent viscosity is not a property of the fluid itself but depends on the dynamic characteristics of the turbulent flow. Modeling the turbulent viscosity from the time-averaged dynamical characteristics of the turbulent flow is the aim of first-order turbulence models that are presented in the next subsection.

2.2. Turbulence models

The choice of the turbulence model largely depends on its ability to represent correctly the different physical phenomena governing the flow. First-order turbulence models, based on the introduction of a turbulent viscosity, are widely used. The closure of the problem is then obtained by using 0, 1, or 2 additional transport equations. In the following subsections, five first-order turbulence models that will be used to simulate the flow around the swimmer are briefly described with their respective advantages and drawbacks. All these models are implemented in the fluent CFD code used to carry out the numerical simulations of this study.

2.2.1. Standard kk–εε model

The standard *k*–*ε* model is the most known of the turbulence models presented in this paper. It is widely used as it offers a good compromise between the numerical effort (CPU time) and the accuracy of the solution. This is a semiempirical model that was first proposed by Launder and Spalding [5]. This model needs to solve two additional transport equations in order to determine the turbulent viscosity. These two additional transport equations concern the turbulent kinetic energy (*k*) and its dissipation rate (*ε*) and are written as follows (Equations 4 and 5):

Standard *k*–*ε* equations:

$$\overline{U_i}\frac{\partial k}{\partial x_i} = \frac{1}{\rho}\frac{\partial}{\partial x_i}\left(\frac{\mu_t}{\sigma_k}\frac{\partial k}{\partial x_i}\right) + P_k - \varepsilon \tag{4}$$

$$\overline{U_i}\frac{\partial \varepsilon}{\partial x_i} = \frac{1}{\rho}\frac{\partial}{\partial x_i}\left(\frac{\mu_t}{\sigma_\varepsilon}\frac{\partial \varepsilon}{\partial x_i}\right) + c_1\frac{\varepsilon}{k}P_k - c_2\frac{\varepsilon^2}{k} \tag{5}$$

with $P_k = \frac{\mu_t}{\rho}\left(\frac{\partial \overline{U}_i}{\partial x_j} + \frac{\partial \overline{U}_j}{\partial x_i}\right)\frac{\partial \overline{U}_i}{\partial x_j}$

The turbulent viscosity is calculated by using the following relationship (Equation 6):

$$\mu_t = \rho\, c_\mu \frac{k^2}{\varepsilon} \tag{6}$$

where C_μ is a constant.

The constants of the standard *k*–*ω* model have been determined from numerous experiments. Their values are summarized in Table 1.

c_μ	c_1	c_2	σ_k	σ_ε
0,09	1,44	1,92	1,0	1,3

Table 1. Constants of the standard k-ε turbulence model

http://dx.doi.org/10.5772/61176

From now on, the standard k–ε model is nearly the only model that was used during CFD simulations of flows in human swimming [1, 3, 6]. Nevertheless, this model presents some weak points such as the simulation of curved boundary layers or vortical flows. Recirculations can hardly be found by this model.

Furthermore, turbulent flows are significantly affected by the presence of a wall (the body surface in the case of a swimmer) where the molecular viscosity plays an important role. Indeed, velocity fluctuations are notably reduced by the effect of the viscosity in the near-wall region, while the standard k–ε model assumes a fully turbulent flow in the whole fluid domain. As a result, a specific treatment of the near-wall region is required to account for the turbulence modifications in the near-wall region when using the standard k–ε model. In the present study, this was done by using the "nonequilibrium wall function."

The above-mentioned limitations of the standard k–ε model are first indications that this model may not be the most appropriate to predict the flow structure around the swimmer. This is the reason why four other first-order turbulence models in order to determine the most suitable model for such a problem can be tested.

2.2.2. RNG k–ε model

This model was derived from the unsteady Navier–Stokes equations by using a statistical mathematical method called "ReNormalization Group" [7]. A new term is added in the dissipation rate (ε) transport equation. In this model, an effective turbulent viscosity is introduced that varies with the effective Reynolds number. The RNG model is similar to the standard model. For high Reynolds numbers, the effective turbulence equation is the same as with the standard k–ε model. However, the additional term carries out a significant improvement in the accuracy of the simulations of flows with abrupt changes of direction or with strong shearing. Furthermore, it allows a better modeling for low Reynolds numbers and near the wall (or body), while the standard k–ε model is more suited to high Reynolds number flows.

2.2.3. Realizable k2.2.3 Realizable k–ε model

The word "realizable" means that this model satisfies some mathematical criteria concerning the Reynolds stresses, logical with the physics of turbulent flows [8]. In this model, the kinetic energy equation is the same as in the standard model, except for the constants, whereas the dissipation rate equation differs. The turbulent viscosity is determined by using the same formula as with the standard model, but the coefficient C_μ is no longer constant and depends on the flow characteristics. This model provides better performances in the case of flow simulations with boundary layers under strong adverse pressure gradients, reticulating zones or separating boundary layers.

2.2.4. Standard k–ω model

This is a model based on two additional transport equations like the standard k–ε model: one for the kinetic energy (k) and the other for the specific dissipation rate (ω) of the turbulence [9].

As previously mentioned, the dissipation rate (ε) is difficult to specify near the wall. Therefore, in order to overcome this difficulty, one may solve the transport equation of another quantity such as ω. The standard k–ω model is well suited to wall-bounded flows and free shear flows.

2.2.5. Spalart–Allmaras model

This model was proposed by Spalart and Allmaras [10]. Unlike the other turbulence models, which express the turbulent viscosity as a secondary unknown, only one transport equation is solved directly and takes into account the effect of the wall in order to determine the turbulent viscosity. This model was specifically designed for applications implying flows limited by walls. This model is well suited for boundary layers subjected to adverse pressure gradients.

2.2.6. Criterion for choosing a turbulence model

The aim of the present section is to specify which turbulence model is the most appropriate for the numerical study of the flow around a swimmer during underwater swimming. The influence of the choice of the turbulence model on the results of the numerical simulations will be examined. Numerical simulations of the flow around the swimmer have been carried out by using the five different turbulence models described in Section 2. The numerical parameters are the same as those used in a previous study [4] except for the meshing. The meshing was refined in the vicinity of the swimmer in order to better visualize the vortical structures developing along the swimmer's body.

One of the criteria used is the numerical simulation of hydrodynamic special areas where vertical structures occur. The reference used comes from experimental visualizations obtained by the tuft method, showing the location of where separation and reattachment of main vortices appears (Figure 1).

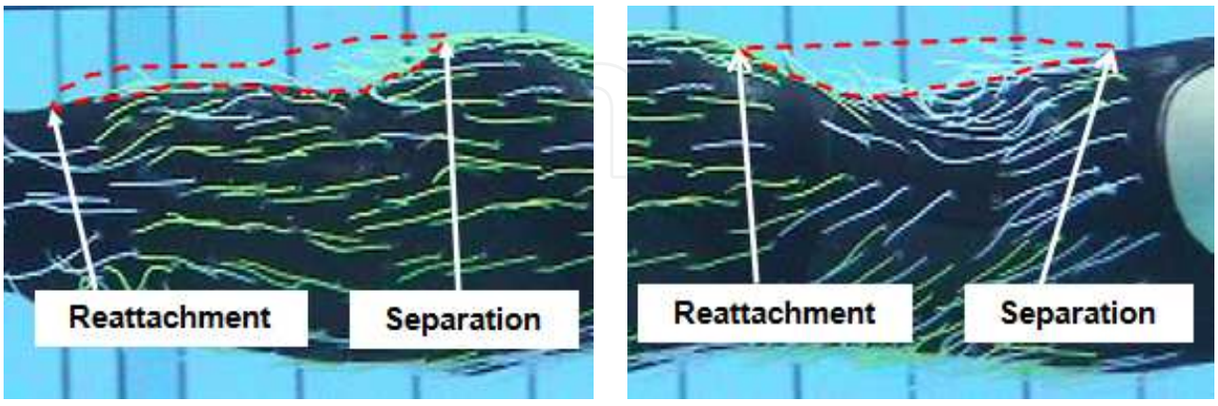

(a) Vortical structure (separation) at the buttocks level.

(b) Vortical structure (separation) at the back level.

Figure 1. Experimental visualizations of vortical structures at the back and buttocks levels during underwater swimming. Swimmer's speed: $U_O = 2.2$ m/s.

http://dx.doi.org/10.5772/61176

Numerical streamline patterns of the resulting flows around the swimmer's head and body are plotted in Figure 2. One may note that all the turbulence models are able to catch three vortical regions around the swimmer's head. Two main large-scale vortices are observed on both sides of the head, especially in the neck and nape regions. One may clearly observe a separation of the flow at the back of the head with its reattachment on the upper part of the back as well as another flow separation starting at the tip of the nose with its reattachment on the breast. A secondary small-scale vortex acting like a junction vortex is present at the arm/head corner, whatever the model used. The presence of this particular vortex is obviously not physically correct; it is only a consequence of the 2D modeling, which considers the arm as a direct extension of the head.

These three regions are very similar in shape and size for the five turbulence models. As a result, it may be concluded that the study of the flow structure around the sole head is not sufficient to assess the efficiency of the turbulence models. Indeed, the locations where flow separations and reattachments occur are imposed by the shape of the head. The similar behaviors noticed around the head for all turbulence models are no longer observed along the body, especially in the back and the buttocks regions. In these regions, one may note large discrepancies among the numerical results obtained with the different turbulence models.

As can be seen in Figure 2, the standard k–ε model provides streamline patterns, indicating a flow that follows closely the shape of the body. No boundary-layer separation and, consequently, no vortical structure are obtained along the swimmer's body. This is in contradiction with the experimental observations given in Figure 1. The vortical structure in the buttocks region has been captured by the four other turbulence models, namely, the RNG model, the realizable k–ε model, the Spalart–Allmaras (SA) model, and the standard k–ω model. However, we may observe that the separation zone behind the buttocks varies as a function of the turbulence model. Three of these models (RNG, realizable, and SA) indicate a smaller separation zone than that visualized during the experiments. As concerns the standard k–ω model, the size of the separation zone at the buttocks level corresponds approximately to that observed experimentally. The locations of the flow separation and of the flow reattachment are very close.

In the back region, turbulence models have more difficulties to find the vortical structures observed experimentally. The standard k–ω is the sole turbulence model that is really able to catch such a structure. The SA model provides only a tiny recirculation zone whereas the two other models (RNG and realizable) are unable to catch any structure in that region. However, the separation zone captured by the k–ω model in the back region remains underestimated by the numerical simulation.

In continuity, Arfaoui et al. [11] have compared the CFD simulations using the standard k–ω turbulence model with the results of experiments by investigating the characteristics of the flow around a female swimmer. The experimental protocol has been performed in the swimming pools of the National Institute of Sports and Physical Education in Paris. Flow visualizations were performed by using the tufts method. The tufts were fixed directly to the swimsuit, and their length was chosen (0.08 m) to highlight the structure of the flow around the swimmer's body and to respond promptly to changes in the direction of the flow with a

specific gravity equal to that of the water ensuring neutral buoyancy. Numerical streamlines reveal that complex turbulent zones were generated, particularly in the regions with sudden changes in the body shape such as head, shoulders, and buttocks. The results of these experiments confirmed the 3D numerical simulations using the standard k–ω turbulence model in CFD.

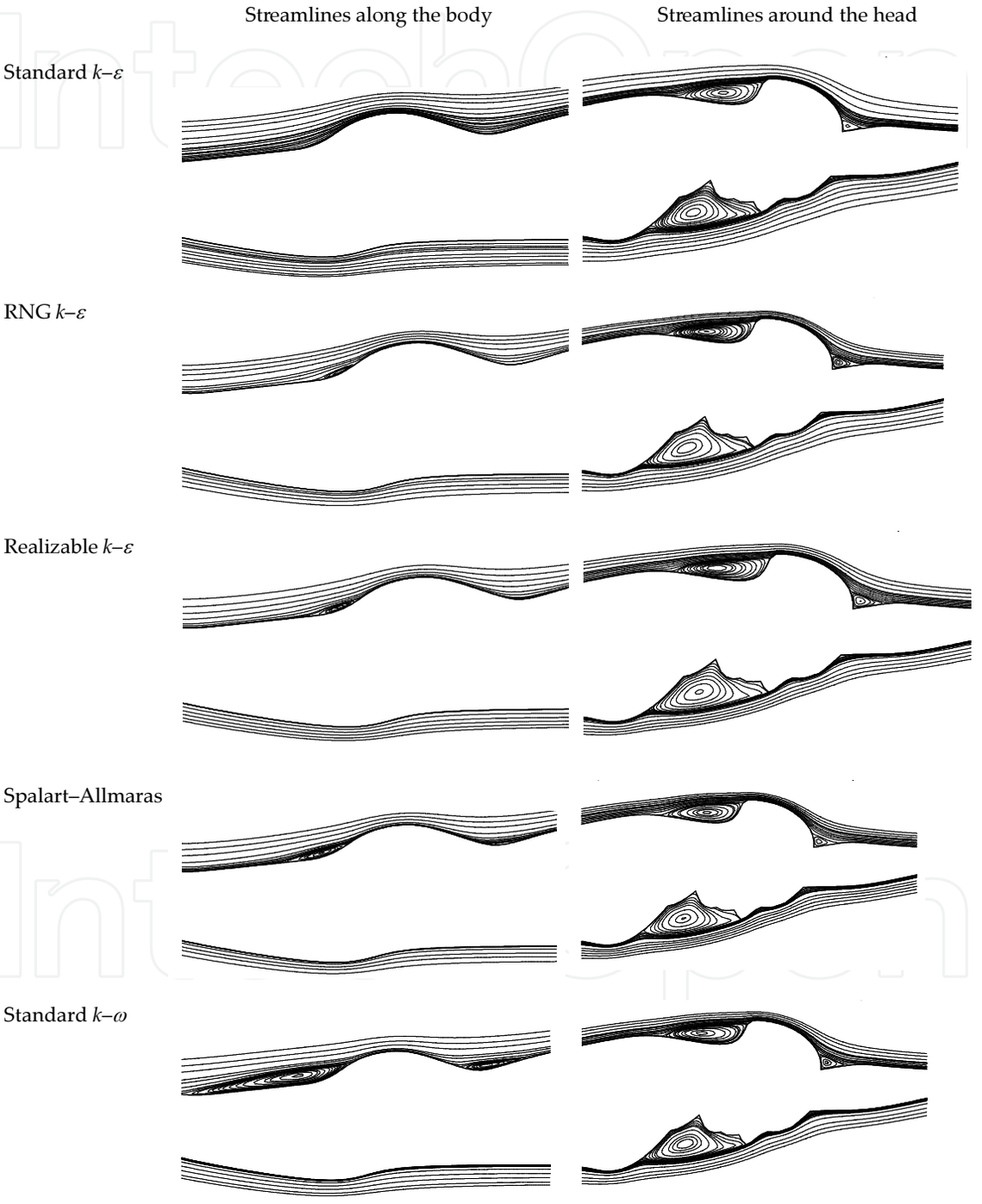

Figure 2. Streamline patterns around the swimmer's body. Swimmer's speed: $U_O = 2.2$ m/s.

http://dx.doi.org/10.5772/61176

3. Numerical approach

3.1. Construction of the swimmer's geometry

Realistic models of swimmers are required for finely studying the vortex flow around body. For this reason, the construction of the 3D geometric model must be meticulous. The first numerical work dedicated to 3D geometry was directed by Lyttle and Keys [12]. The objective was to prescribe the elite swimmers a stroke technique optimally feet starting phase "casting" and phase back after the turn to improve the thrust. To do this, they have chosen a high-level swimmer as a model for this study. Building the model of the swimmer has been performed using a 3D scanner "WBX Cyberware" high resolution, and the geometry has been constructed at once to a position corresponding to the sliding stage with a shaped body and arms outstretched.

In 2010, Zaïdi et al. [13] studied a national-level female swimmer model for their numerical simulation. The construction of the 3D geometric was conducted by a Konica Minoltas scanner (Figure 3).

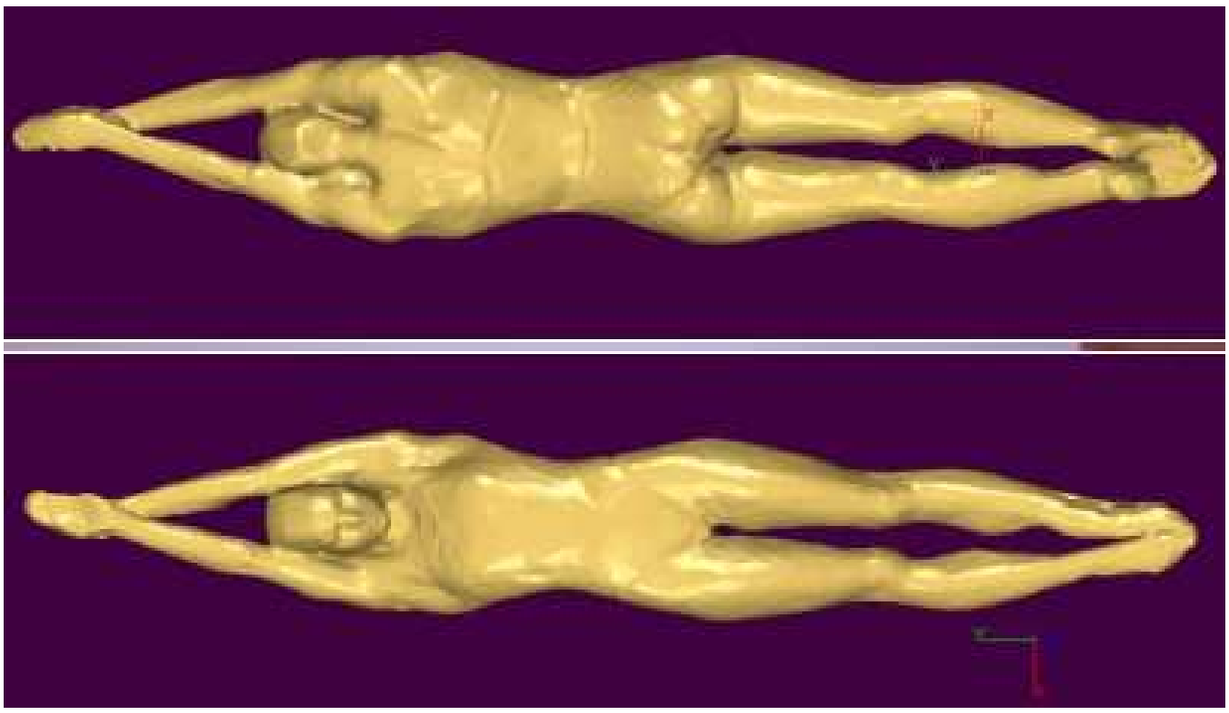

Figure 3. Geometry of the female swimmer obtained from a laser scan.

3.2. Construction of the fluid domain around the swimmer

After constructing the swimmer's geometry, the next stage consists in building the fluid domain around the swimmer. The dimensions of the fluid field around the swimmer are

chosen so as to ensure the independence of the numerical results. In numerical simulation, the choice of the size of the computational domain plays an important role on the fidelity of numerical results. It must be large enough to overcome the influence of the boundaries of the fluid field on the flow. If the swimmer is placed very close to the entrance, it disturbs the flow and imposes a speed profile unreal to the surface of the swimmer. If it is placed very close to the exit, it prevents the establishment of the flow and deteriorates the performance. Numerical simulations on areas of different sizes have been carried out in order to specify the size of the fluid domain necessary to ensure the independence of the numerical results.

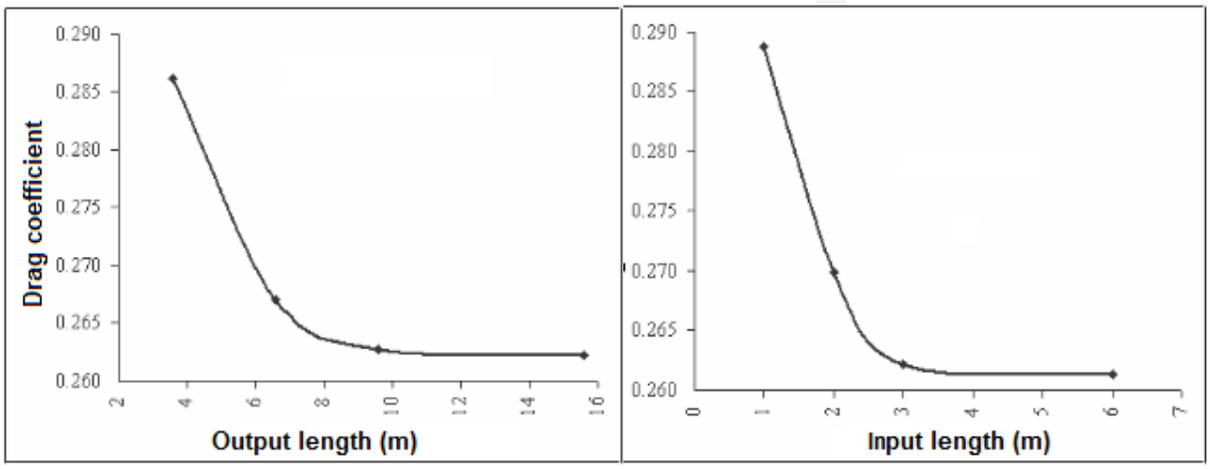

Figure 4. Front and back of the swimmer geometry obtained from a laser scan of the athlete.

In order to ensure the independence of the results from the output and the output length, Zaidi et al. (2008) varied the input and output lengths to avoid their effects on the independence of the numerical results, and they have carried out simulations for such various lengths. They have shown that the drag coefficient becomes stable from 3.0 m of the inlet and one of a distance of 9.6 m from the outlet (Figure 4).

3.3. Grid of the fluid domain

In numerical modeling, the grid of the area plays a leading role on the reliability of the results. The choice of this meshing depends on the expected accuracy of the calculation and the available computing resources. Using a coarse mesh gives erroneous results, while a fine meshing increases the computing time and requires a lot of storage capacity when processing results. The purpose is to find a mesh that occupies less space and time and provides independent results. To assess the influence of the fineness of the mesh on the results, calculation series were conducted to mesh sizes. All tested meshes are progressive, that is to say refined near the surface of the swimmer and released away from the latter. In the study by Zaidi et al. [13], the mesh of the fluid was realized by TGrids software. The mesh was refined near the swimmer and less refined elsewhere so to reduce the computational time.

http://dx.doi.org/10.5772/61176

Figure 5 shows the surface meshing of the swimmer's body and a cross section of the fluid around the swimmer. When a nonstructured grid is used, the flow is not lined up with the grid cells.

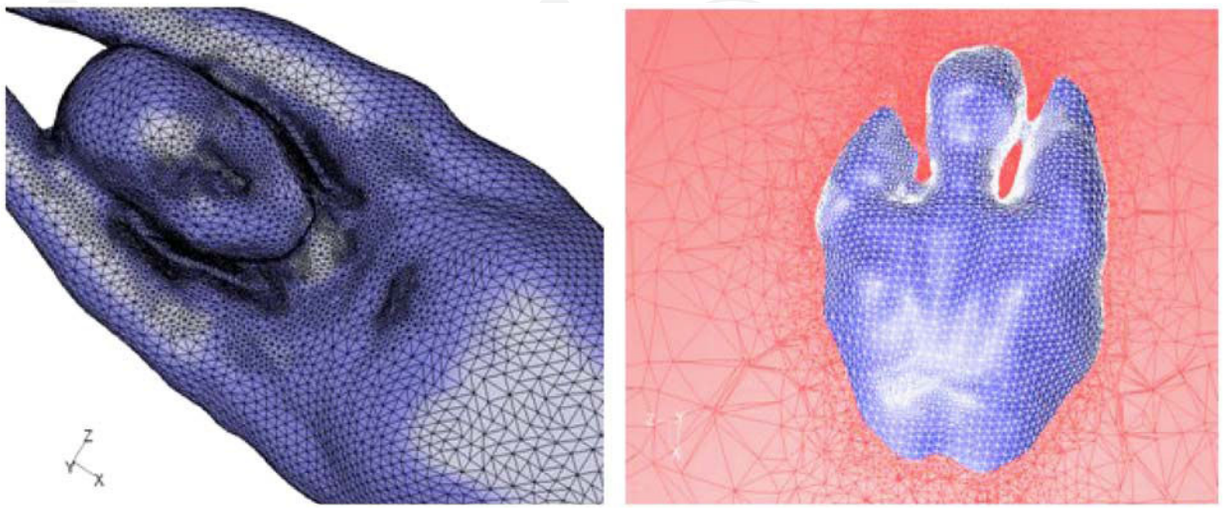

Figure 5. Body surface grid (left) and view of the fluid progressive grid in a plane around the swimmer's body (right).

3.4. Boundary conditions

Once the geometry and meshing defined, it is necessary to choose the geometric areas on which one may apply the boundary conditions used in the numerical simulation. The choice of boundary conditions corresponds to the real problematic. Indeed, special attention should be turned toward the understanding of swimmer's movement in the water.

Popa et al. [14] studied the flow dynamics around a competitive swimmer during underwater glide phases occurring at the start and at turns. The problem is considered as 3D and in steady hydrodynamic state. Three velocities (1.4 m/s, 2.2 m/s, and 3.1 m/s) that correspond to interregional, national, and international swimming levels were studied (Figure 6). The boundary conditions used for the numerical simulations In the study of Popa et al. are :

- At the entrance of the fluid domain: They chose a uniform velocity profile.
- At the exit of the fluid area: They chose mass conservation law.
- On left, right, upper and lower limits of the fluid domain: They chose the condition of symmetry is imposed. Symmetry boundary conditions are used to model zero-shear slip walls in viscous flows and to avoid the boundary layers that develop on the walls of the domain and which are not real.
- On the surface of the swimmer: The no-slip condition is used.

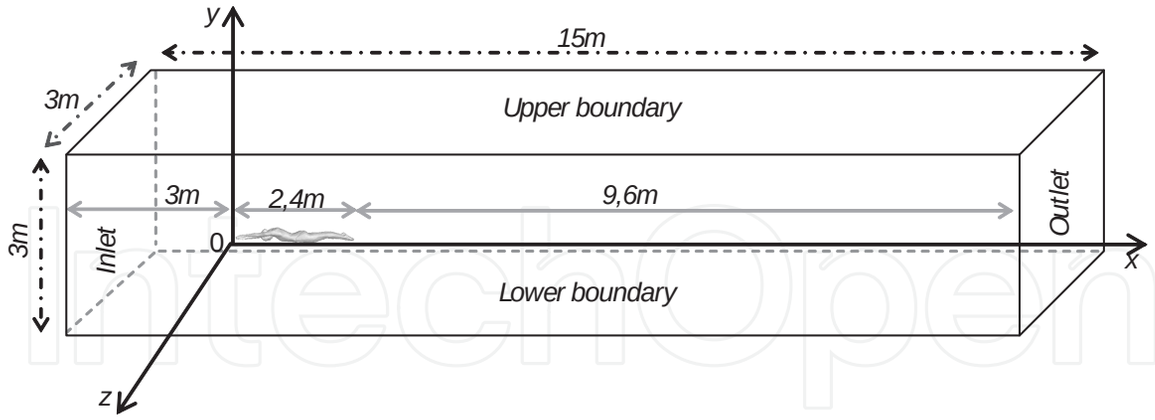

Figure 6. View of the external boundaries of the fluid area around the swimmer.

4. Hydrodynamic drag forces

Numerical simulations of the flow around a swimmer during the different swimming phases were carried out to understand the drag force. In mechanics of swimming, the reduction of drag forces opposed to the swimmers movement plays an important role in the improvement of the performances. For this reason, optimization of the position and movement of the swimmer is necessary in order to determine the optimal parameters that correspond to the minimal drag forces. The total resistance, also called total drag, is composed by three main components:

- Viscous drag or friction due to the viscosity of the fluid medium pressure
- Pressure drag, mainly due to the complex shape of the human body
- Wave drag caused by the wave field that accompanies the moving body and extending gradually over a considerable area of the free surface [15–18].

The pressure drag and the viscous drag depend on the Reynolds number.

In fluid dynamics, the drag equation is as follows:

$$F_D = \frac{1}{2}\rho u^2 C_D A \tag{7}$$

where F_D is the drag force: force component in the direction of the flow velocity; ρ is the mass density of the fluid; u is the flow velocity relative to the object; C_D is the drag coefficient—a dimensionless coefficient related to the object's geometry; and A is the reference area.

The reference area A is typically defined as the area of the orthographic projection of the swimmer on a plane perpendicular to the direction of motion.

http://dx.doi.org/10.5772/61176

Rouboa et al. [3] used a turbulent model to calculate the drag and lift coefficients of the hand/forearm both under steady and unsteady flow conditions. They determined the effect of the acceleration of the hand/forearm on the generation of the propulsive force. Sato and Hino [2] carried out unsteady CFD simulations in order to consider the effects of acceleration and transient motions of the hand in predicting swimmer's thrust. Gardano and Dabnichki [6] estimated the hydrodynamic drag and lift forces. Their work constituted an important projection toward the use of CFD in the simulation of swimming in unsteady regime.

The contribution of these three drag forces in swimming varies depending on both swimming speed and depth. According to Rushall et al. [17], a doubling of swimming speed increases twice the friction drag, four times the drag, and eight times the wave drag. Toussaint et al. (2002) assumed that for a swimming speed of 1 m/s, contributions of the three drag components in the total drag are 3% for the friction drag, 95% for the form drag, and 2% for the wave drag. These values respectively become 3%, 77%, and 20% at a speed of 2 m/s. They also indicate that the contribution of the friction drag does not exceed 5% of the total drag. An increased wave drag increases the form drag, while the friction drag is considered independent of the first two. The two streaks of form and wave are dependent. Increasing wave drag increases the form drag, while the friction drag is considered independent of the drag of form and wave.

In order to analyze the effect of the position of the swimmer's head on the hydrodynamic performances in swimming and in evolution of drag, Zaïdi et al. [4, 19] neglected wave drag because the underwater glide phases occurring at the start and at turns were placed away from the free surface (the swimmer is placed at a depth of 1.5 m) [16, 20].

Figure 7 shows the variation of the pressure, viscous, and total drag forces calculated for the three head positions and for velocities ranging between 1.4 and 3.1 m/s. One may observe that the position of the head aligned with the body (position 2) is the one that offers less resistance. In the case of position 2 and for a speed of 3.1 m/s, the viscous drag accounts for 20% whereas the form drag accounts for 80% of the total drag.

The curves show that a change in the head position induces an important modification of the total drag in the velocity range of 1.4 to 3.1 m/s. The total drag vary from 4% according to the head position and this whatever the speed of the swimmer. This difference in drag is very important in high-level competition.

4.1. 2D versus 3D modeling

In complex problem of fluid dynamics where complex phenomena occur, many restrictions were noted in the use of 2D modeling. The 2D study is insufficient and the 3D study seems inevitable to be able to model vortex structures and separation areas.

Figure 8 shows comparison between the numerical results of a 3D study with the k–ω model and the 2D study carried out by Zaïdi et al. [4, 19] using both the k–ε and the k–ω turbulence models. On the same Figure 8, the 3D experimental results obtained by Bixler et al. [21] and Vennell et al. [16] are also presented. The 2D study appears to be limited as it does not enable to evaluate correctly the drag forces, and that the 2D study is unavoidable in swimming analysis. Indeed, the total drag values calculated in the case of the 2D study are much higher

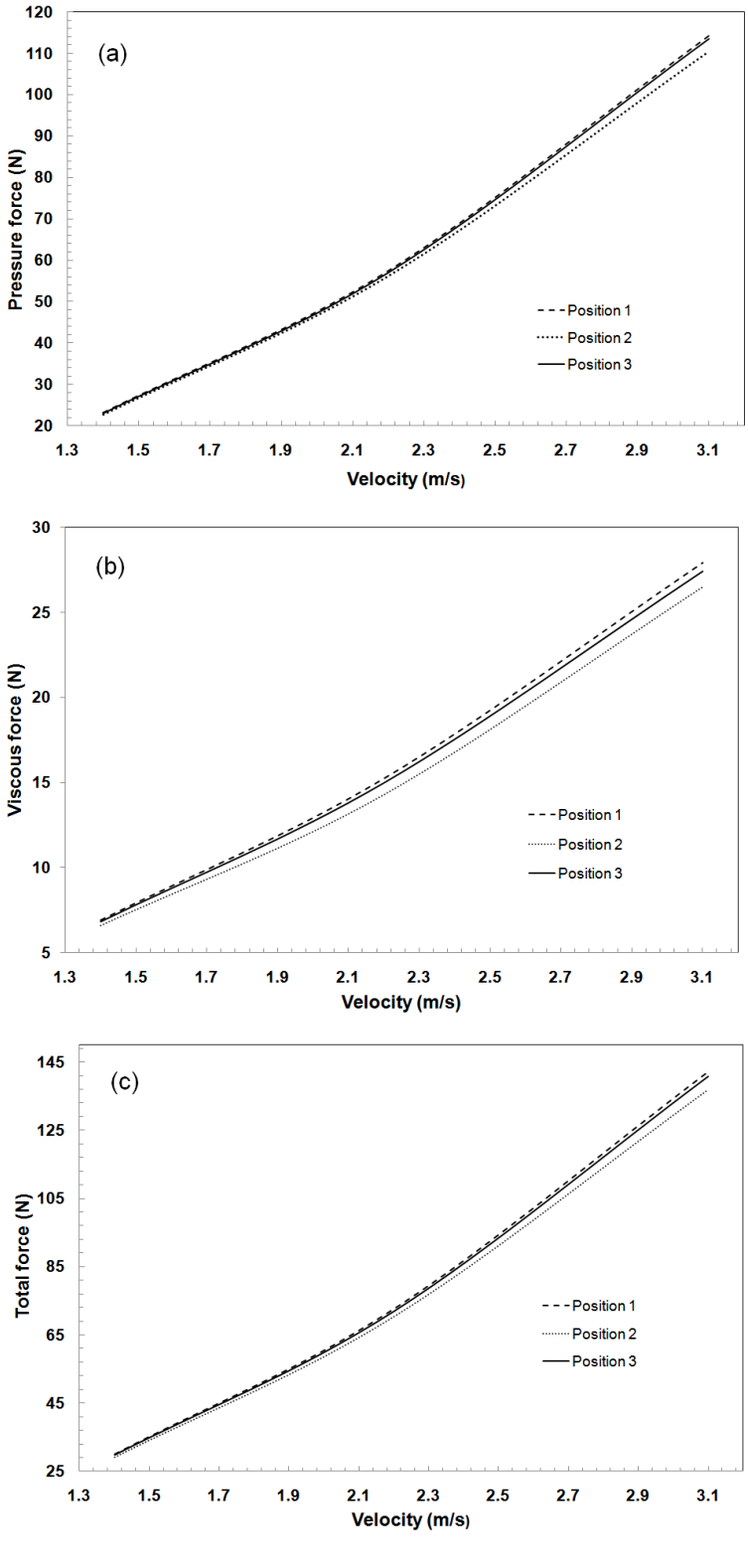

Figure 7. Evolution of the pressure (a), viscous (b), and total (c) force as a function of the head position and velocity.

than the ones calculated in the case of the 3D study, whatever model of turbulence has been used.

http://dx.doi.org/10.5772/61176

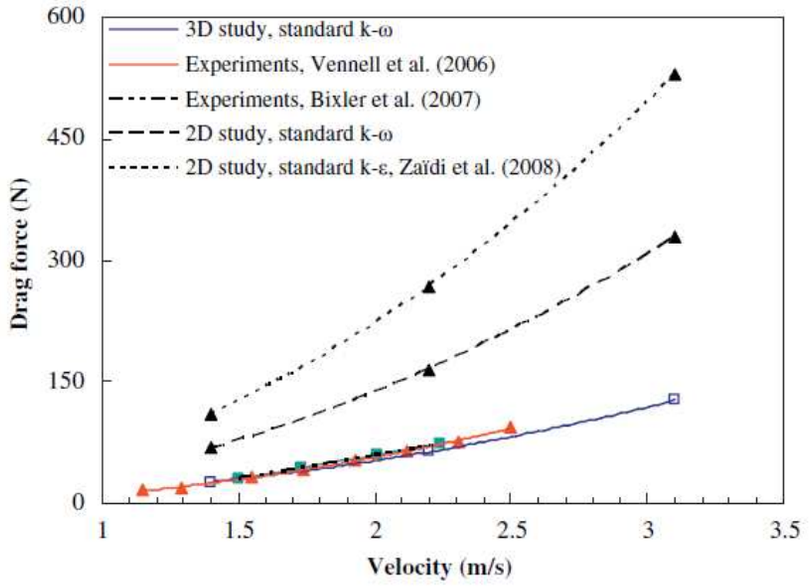

Figure 8. Comparison between the experiments of Vennel et al. [16, 19] and the 2D and 3D numerical results.

4.2. Position influence

Several authors carried out measurements on the whole body of the swimmer and estimated the influence of various parameters such as the swimmer's position or morphology on the intensity of the drag [22]. Other investigators studied the effect of the hand/forearm position on the propulsion effect of a swimmer [23]. Berger et al. [24] measured the drag and lift forces on two hand/forearm models by using the quasi-static approach. The results were compared for velocities, various sizes, and orientations. Bixler and Riewald [1] were the first who used the CFD method to simulate the water flow around a swimmer's hand and forearm (Figure 9). They estimated the drag forces and coefficients around a swimmer's hand and forearm for different angles of attack.

Rouboua et al. [3] have calculated numerically the drag and lift coefficients for a swimmer's hand and forearm in both the steady- and the unsteady-state cases. They studied the effect of the acceleration of the hand and forearm on the generation of the propulsion force. Gardano et al. [6] have also calculated numerically the importance of the flow analysis around the whole arm of a swimmer, and they have estimated the propulsion and the drag forces. More recently, the numerical results obtained by Zaïdi et al. [4] in a 2D geometry case have revealed that the position of the head had a noticeable effect on the hydrodynamic performances. The analysis of these results made it possible to propose an optimal position of the swimmer head in underwater swimming.

In this section, numerical simulations of the flow around a swimmer during underwater swimming corresponding to the starting phase (after the start dive) or following a turn are presented. The aim is to optimize the performance among high-level swimmers by reducing drag effects considering the position of the swimmer's head. Three positions of the head are investigated: lifted up, aligned, or lowered. The length of the swimmer, with arms and hands

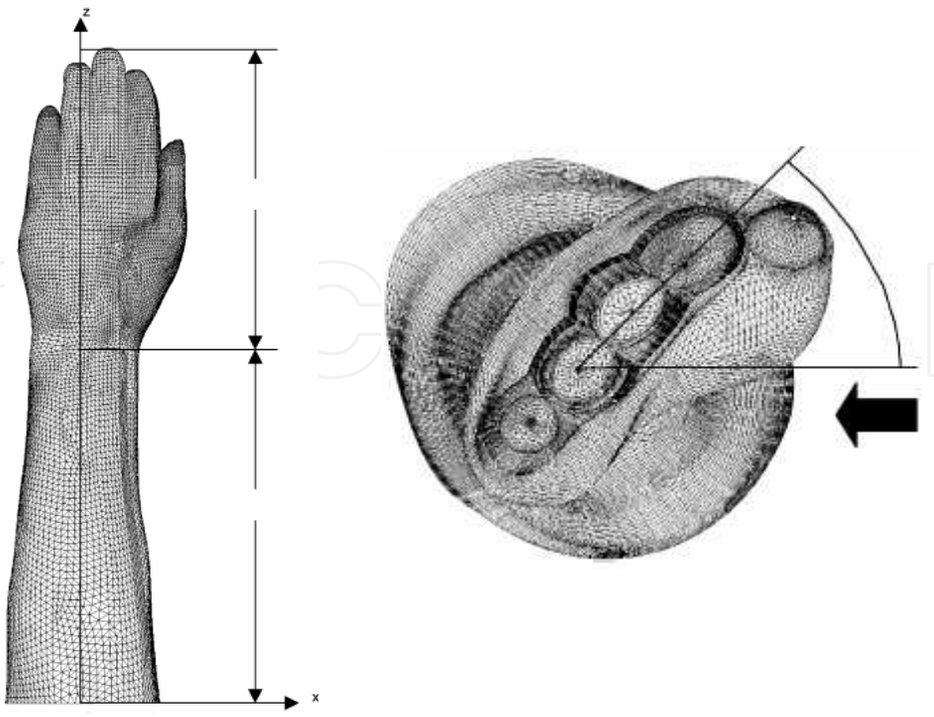

Figure 9. CFD surface mesh of hand and arm with coordinate system [1] and angle of attack defined.

outstretched corresponding to the position of the swimmer in the underwater starting phase, is 2.4 m. In this study, three positions of the head have been investigated: lifted up, aligned, and lowered corresponding to positions 1, 2, and 3 schematized in Figure 10. Only the head modifies the general posture.

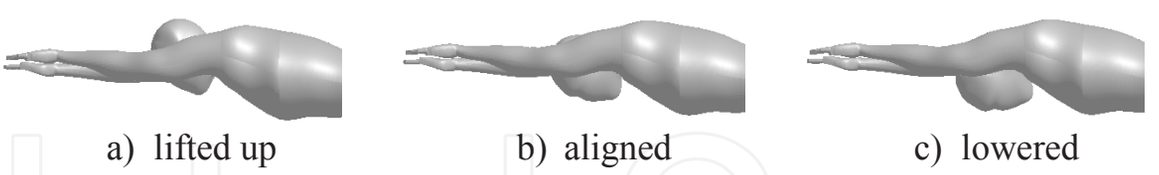

Figure 10. Positions of the head.

5. Streamline patterns

Improving the swimming performance leads also to understand the behavior of the water circulating around the swimmer. A swimmer in streamlined position will not generate the same wake as a swimmer in an unoptimized position. The vortex structures will differ in size and position, as well as areas of vortex separation and attachment. Collapse near this wake allows to reduce the drag force and thus to enhance the performance. In such a way, CFD is a powerful tool to study the flow around swimmers as it avoids making for very complicated

http://dx.doi.org/10.5772/61176

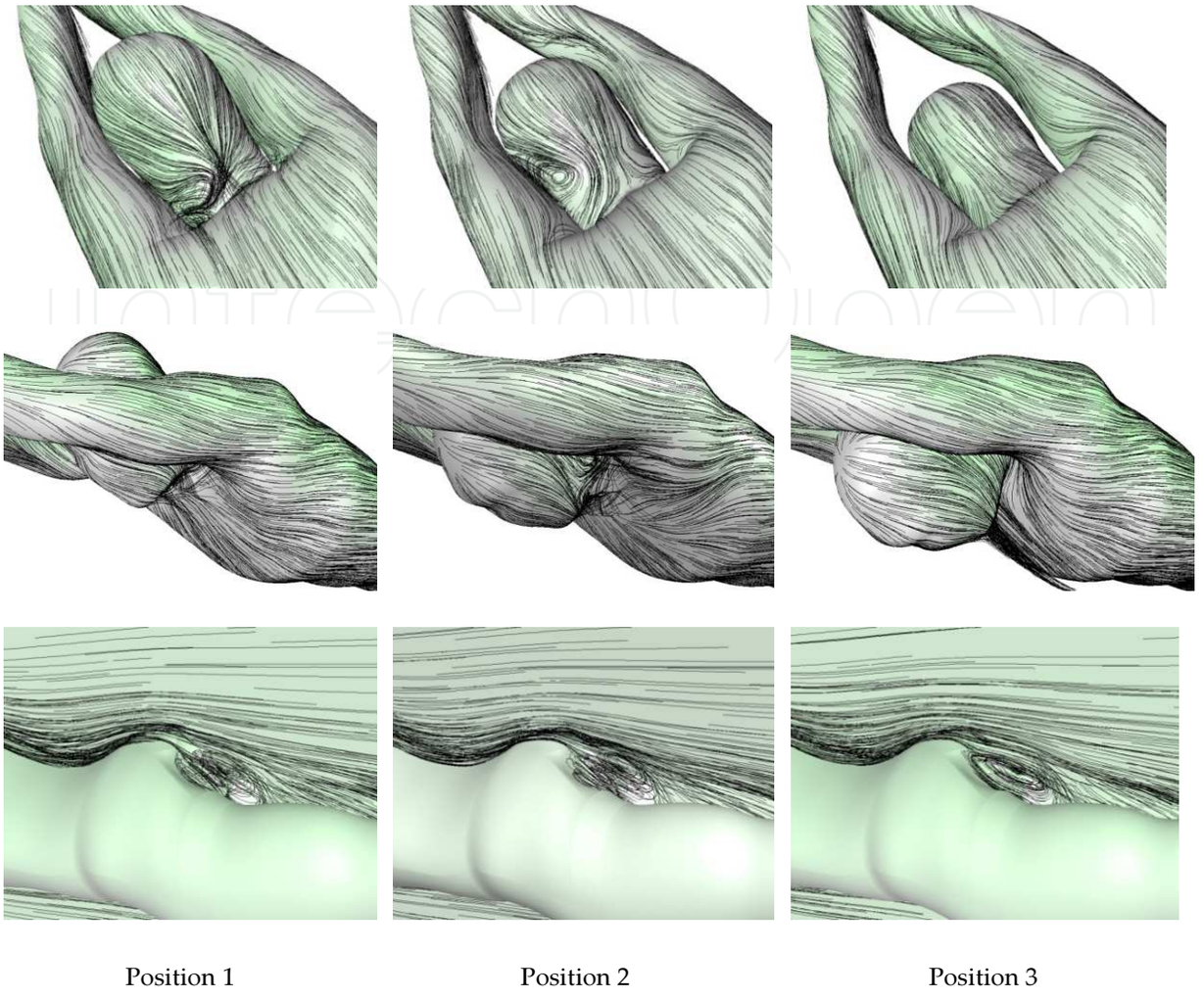

Figure 11. Streamline patterns around the swimmer for three head positions and U_0 = 3.1 m/s [26].

experiments to achieve. Because of the nonuniformity and complexity of the human body, complex turbulent zones are generated around the swimmer's body [20], particularly in the regions with sudden changes in the body shape such as head, shoulders, elbows, hips, knees, buttocks, and feet [25].

Popa et al. [26] showed in Figure 11 streamline patterns to highlight the flow structure around the swimmer's neck, chin, and buttocks for each of the three head positions and for a velocity of 3.1 m/s. One may observe recirculation zones around the swimmer's neck, chin, and buttocks according to the position of the head. For example, when the head is lifted up or aligned with the body, two upper and lower separated points induce vortices.

One may note that these closed vortices are located in the concave geometry of the body, namely, the nape of the neck for the upper surface and the chin/breast area for the lower surface. On the contrary, for the position of the head lowered (position 3), there is no recirculation zones in the neck or under the chin. Because of the nonuniformity of the body on the swimmer's head, shoulders, elbows, hips, knees, and buttocks, complex turbulent zones are

generated around the swimmer's body. In this study, Popa et al. [26] noted a recirculation zone on the swimmer's buttocks with a larger recirculation zone when the head is lifted up whatever the head position. The numerical results show that the position of the head plays a very important role for high swimming velocities on the hydrodynamic performances. The position of the head aligned with the body is the one that offers less force drag in comparison with positions with head lowered or lifted up. Complex turbulent zones due to the nonuniformity of the human body are generated around the swimmer's body. This occurs particularly in the regions with sudden changes in the body shape such as the chin, neck and buttocks when the head is lifted up or aligned.

6. Velocity profiles and wall shear stress

The resistance force of advancement strongly depends on the pressure fields and the wall shear stress around the swimmer. The performance improvement requires a better understanding of the structure of the fluid flow around swimmers and a good knowledge of the pressure fields and wall shear stress encountered to minimize them.

Wall shear stress and static pressure are fundamental parameters in high-level swimming. When a swimmer moves in the aquatic environment because of the nonuniformity and complexity of the human body, negative pressure gradients and turbulence zones are generated around the swimmer's body [20], particularly in the regions where the body suddenly changes shape as head, shoulders, elbows, hips, knees, and feet [25].

In the study of Popa et al. [14], the wall shear stress increases with the velocity and consequently the resistance force of advancement increases as well. Also, the wall shear is important in the areas where the body shape suddenly changes, such as the head, the shoulders, the buttocks, the heel, and the chest. Figures 12 and 13 represent the surface shear stress on the swimmer's body for three positions of the head, namely, lifted up (position 1), aligned (position 2), and lowered (position 3) in back and front views. To achieve this, they have chosen a high velocity (u_0 = 3.1 m/s) that corresponds to an international level swimmer. The wall shear stress is higher behind the head for position 1 (Figure 12(a)) and on the forehead in position 3 (Figure 13(c)). Figures 14 and 15 present the back and front views of the pressure field for each of the three head positions and u_0 = 3.1 m/s. They observed the negative pressure gradients behind the head for position 1 (Figure 14(a)) and on the forehead in position 3 (Figure 15(c)), which indicate that there are separation zones in these areas.

In a previous study, Zaïdi et al. [19] have found that the position of the head aligned is the one that offers less resistance in underwater swimming in comparison with the positions of the head lifted up and lowered. The pressure gradient between the different parts of the swimmer generates a resistance force that acts perpendicular to the surface of the body which slows the swimmer [17]. The more the resistance force to the advancement, the more wall shear stress observed. The wall shear stress increases with velocity and consequently the resistance force to advancement increases. Also, the wall shear stress is important in the regions where the body shape suddenly changes, such as the head, the shoulders, and the buttocks. In these regions, flow separations occur and the pressure decreases sharply.

http://dx.doi.org/10.5772/61176

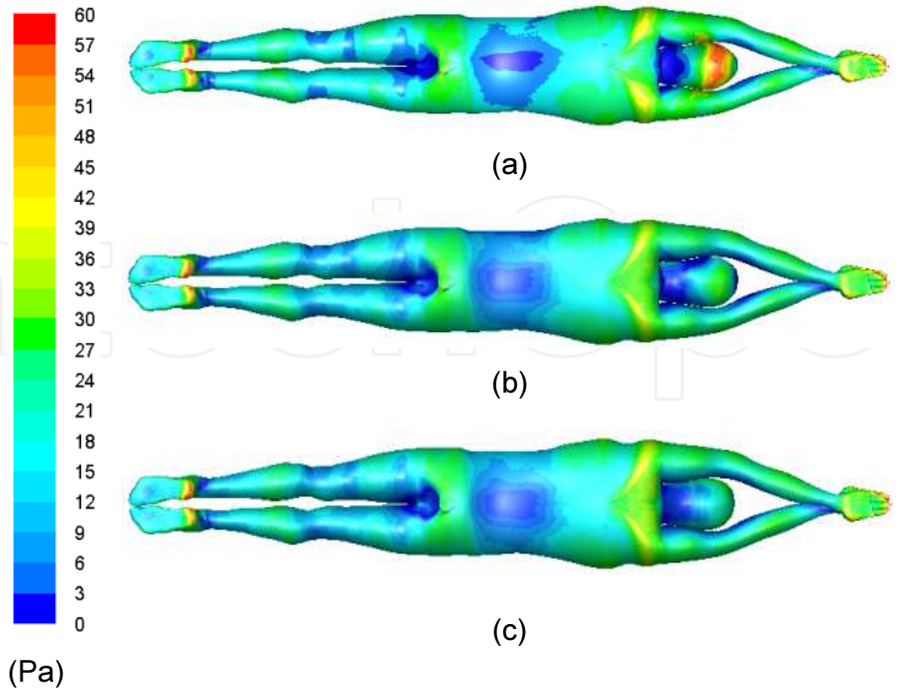

Figure 12. Wall shear stress for three head positions (lifted up, aligned, and lowered) and U_0 =3.1 m/s on the back view of the swimmer (Popa et al. [14]).

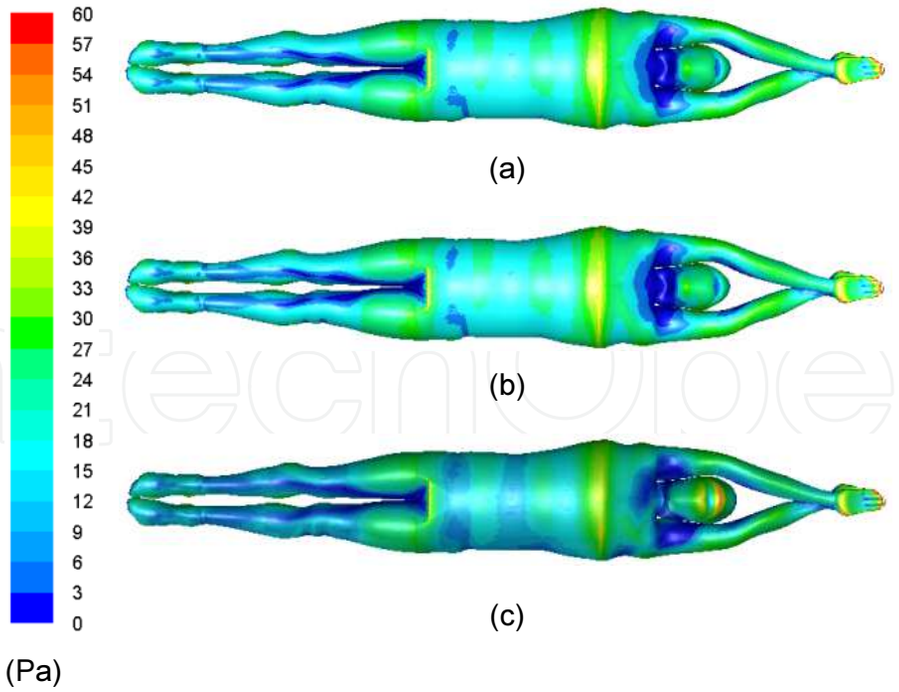

Figure 13. Wall shear stress for three head positions (lifted up, aligned, and lowered) and U_0 =3.1 m/s on the face view of the swimmer (Popa et al. [14]).

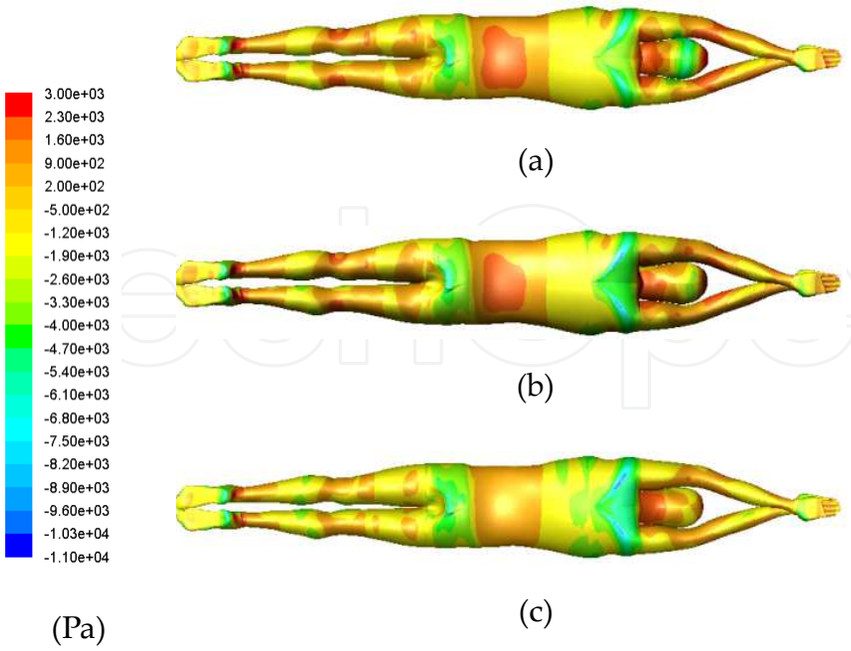

Figure 14. Pressure field for three head positions (lifted up, aligned, and lowered) and U_0 =3.1 m/s on the back view of the swimmer (Popa et al. [14]).

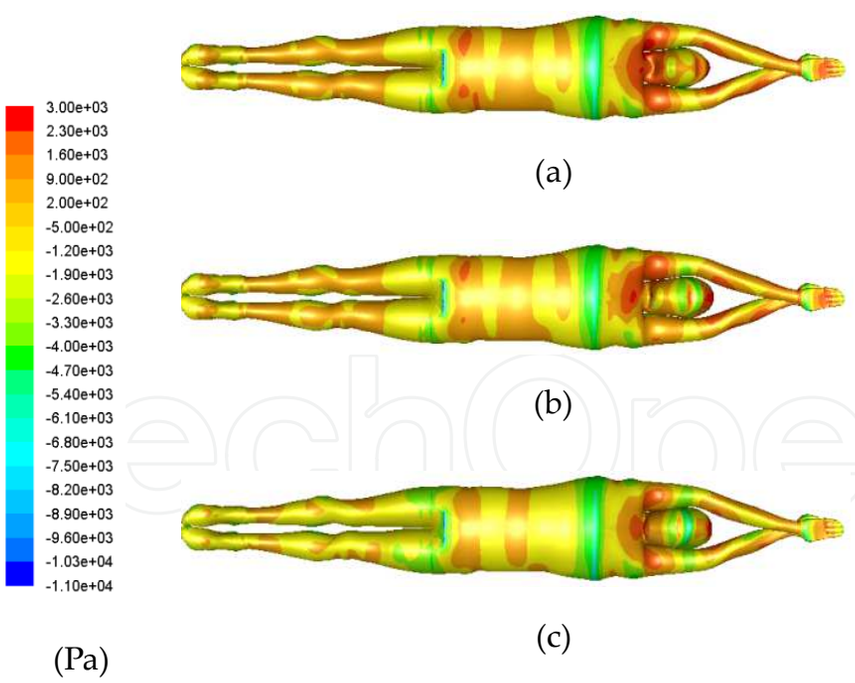

Figure 15. Pressure field for three head positions (lifted up, aligned, and lowered) and U_0 =3.1 m/s on the face view of the swimmer (Popa et al. [14]).

To consolidate these findings, Popa et al. [26] studied the dimensionless longitudinal velocity profiles plotted for six plane locations, for the three positions of the head and for U_0 = 2.2 m/s.

http://dx.doi.org/10.5772/61176

Note that the aspect of the velocity profiles along the body is strongly affected by the change in the head position (Figure 16(a) and (b)).

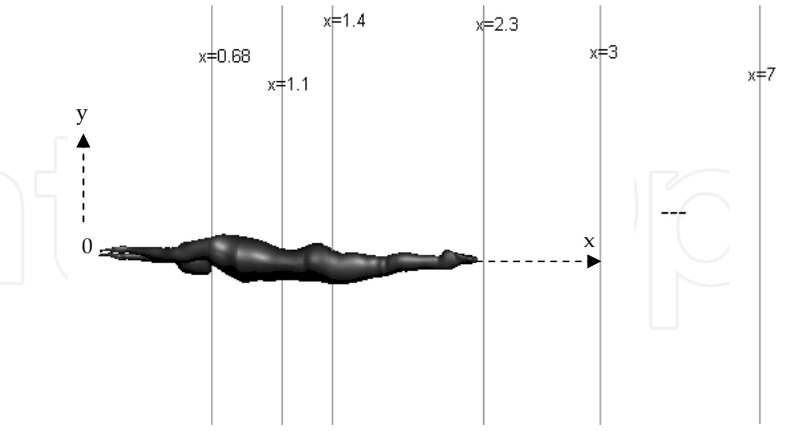

(a)

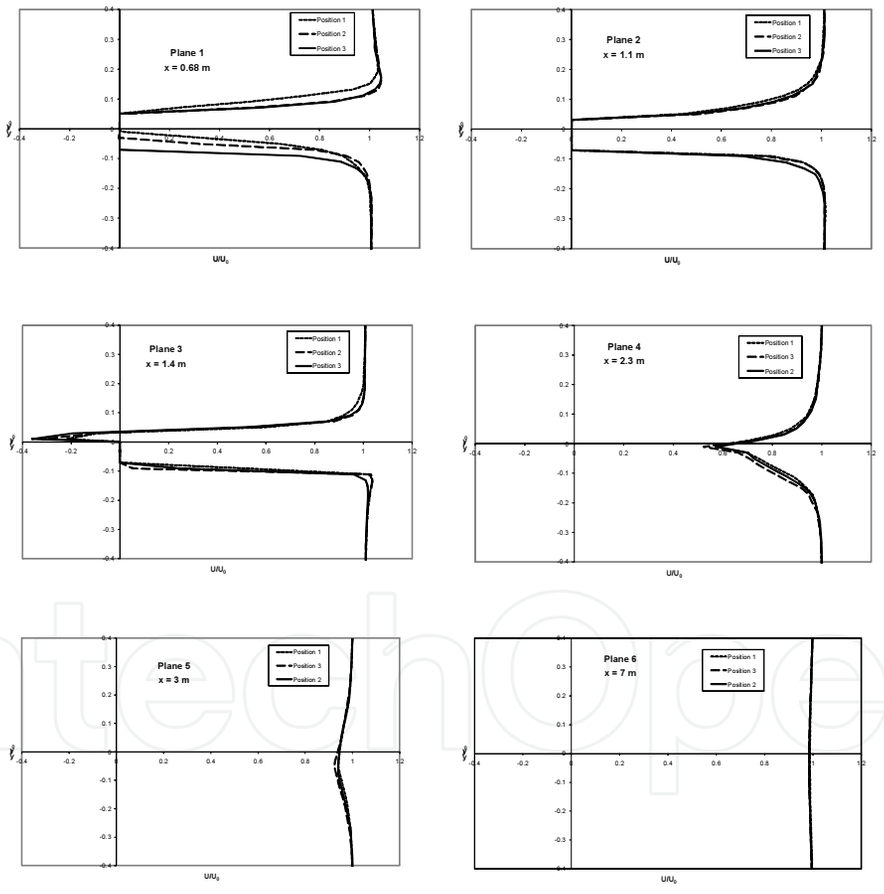

(b)

Figure 16. (a). Planes position in the fluid domain ($z = 0$) from Popa et al. [26]. (b). Dimensionless longitudinal velocity profiles in planes 1–6 for $U_0 = 2.2$ m/s (Re = 6.4 × × 10^6) from Popa et al. [26].

On plane 1, a pronounced increase is noted in the velocity at the upper body surface for lowered and aligned head positions. However, the velocity is greater for lifted up head position. On

plane 2, located at the trunk, there are no differences between the three head positions. In the buttock area (plane 3), at $0 < y/y_0 < 0.04$, negative velocities were observed irrespective of the head positions. This indicates that there are recirculation zones in the buttock area that have the same width. In plane 3, the maximum longitudinal velocity is 40% higher for the third head position (lowered) compared to the first head position (lifted up).

In the wake zone, downstream the swimmer, a deceleration of the fluid is noted (loss of kinetic energy). The differences between the velocity profiles in the wake zone characterize the velocity deficit. This dimensionless longitudinal velocity profiles reveals the importance of the head position in the dynamics of the flow in underwater swimming phases (start dive or turns).

7. Conclusion

The main objective of this work was the numerical study of flow around swimmers to improve their hydrodynamic performance. The performance improvement requires a better understanding of the structure of the fluid flow around swimmers and a good knowledge of mechanics of swimming. This chapter focuses on computational fluid dynamics (CFD) procedures and results for this practical implication in swimming and aims to give more details on numerical models. We may note that the CFD can be used as a powerful tool in swimming understanding if the boundary conditions are well studied and chosen. The study of the flow features around the swimmer during the different swimming phases showed that the reduction of forces, which oppose to the swimmers advancement, plays great importance part in the improvement of the performances.

Author details

Ahlem Arfaoui[1*] and Guillaume Polidori[2]

*Address all correspondence to: ahlem.arfaoui@univ-reims.fr

1 Biomechanics Team/Research Group in Engineering Sciences (GRESPI EA4694), University of Reims, France

2 Thermomechanics team/Research Group in Engineering Sciences (GRESPI EA4694), University of Reims, France

References

[1] Bixler, B., Riewald, S., 2002. Analysis of swimmer's hand and arm in steady flow conditions using computational fluid dynamics. Journal of Biomechanics 35, 713–717.

[2] Sato, Y., Hino, T., 2002. Estimation of Thrust of Swimmer's Hand Using CFD National Maritime Research Institute, Center for CFD Research, Shinkawa 6-38-1, Mitaka, Tokyo 181-0004, Japan.

[3] Rouboa, A., Silva, A., Leal, L., Rocha, J., Alves, F., 2006. The effect of swimmer's hand/forearm acceleration on propulsive forces generation using computational fluid dynamics. Journal of Biomechanics 39, 1239–1248.

[4] Zaïdi, H., Taïar, R., Fohanno, S., Polidori, G., 2008. Analysis of the effect of swimmer's head position on swimming performance using computational fluid dynamics. Journal of Biomechanics 41, 1350–1358.

[5] Launder, B. E., Spalding, D. B., 1972. Lectures in Mathematical Models of Turbulence. Academic Press, London, England.

[6] Gardano, P., Dabnichki, P., 2006. On hydrodynamics of drag and lift of the human arm. Journal of Biomechanics 39, 2767–2773.

[7] Choudhury, D., 1993. Introduction to the Renormalization Group Method and Turbulence Modeling. Fluent Inc. Technical Memorandum TM-107.

[8] Shih, T.-H., Liou, W. W., Shabbir, A., Yang, Z., Zhu, J. A., 1995. New k–ε eddy-viscosity model for high Reynolds number turbulent flows. Model development and validation. Computers and Fluids 24, 227–238.

[9] Wilcox, D. C., 1998. Turbulence Modeling for CFD. DCW Industries, Inc., La Canada, California.

[10] Spalart, P., Allmaras, S., 1992. A one-equation turbulence model for aerodynamic flows. Technical Report AIAA-92-0439, American Institute of Aeronautics and Astronautics.

[11] Arfaoui, A., Popa, C.V., Taiar, R., Polidori, G., Fohanno, S., 2012. Numerical streamline patterns at swimmer's surface using RANS equations. Journal of Applied Biomechanics, 28 (3), 279–283.

[12] Lyttle, A., Keys, M., 2004. The use of computational fluids dynamics to optimize underwater kicking performance. In Proceedings of the XXIInd International Symposium on Biomechanics in Sports (p. 403–411). Ottawa, Canada: Imprimerie Impression.

[13] Zaïdi, H., Taïar, R., Fohanno, S., Polidori, G., 2010. Turbulence model choice for the calculation of drag forces when using the CFD method. Journal of Biomechanics 43, 405–411.

[14] Popa, C.V., Zaidi, H., Arfaoui A., Polidori, G., Taïar, R., Fohanno, S., 2011. Wall shear stress analysis around a competitive swimmer using 3D Navier–Stokes equations in CFD, Acta of Bioengineering and Biomechanics 13(1), 3–11.

[15] Polidori G., Taïar R., Fohanno S., Mai T.H. Lodini A., 2006. Skin-friction drag analysis from the forced convection modeling in simplified underwater swimming. Journal of Biomechanics 39, 2535–2541.

[16] Vennel, R., Pease, D., Wilson, B., 2006.Wave drag on human swimmers. Journal of Biomechanics 39, 664–671.

[17] Rushall, B. S., Holt, L. E., Sprigings, E. J., Cappaert, J. M., 1994. A re-evaluation of forces in swimming. Journal of Swimming Research 10, 6–30.

[18] Sheehan, D. P., Laughrin, D. M., 1992. Device for qualitative measurements of hydrodynamic drag on swimmers. Journal of Swimming Research 8, 30–34.

[19] Zaïdi, H., Taïar, R., Fohanno, S., Polidori, G., 2009.An evaluation of turbulence models in CFD simulations of underwater swimming. Series in Biomechanics 24, 5–14.

[20] Lyttle, A.D., 1999. Hydrodynamics of the Human Body During the Freestyle Tumble Turn. Published doctoral dissertation, The University of Western Australia, Nedlands, Australia.

[21] Bixler, B., Pease, D., Fairhurst, F., 2007. The accuracy of computational fluid dynamics analysis of the passive drag of a male swimmer. Sports Biomechanics 6, 81–98.

[22] Huijing, P.A., Toussaint, H.M., Clarys, J.P., Groot, G., de., Hollander, A.P., Vervoorn, K., Mackay, R., Savelberg, H.H.C.M., 1988. Active drag related to body dimensions. In: B.E. Ungerechts, K. Reischle, K. Wilke (Eds.), Swimming Science V, 31–37. Champaign, IL: Human Kinetics Books.

[23] Schleihauf, R.E., 1979. A Hydrodynamic Analysis of Swimming Propulsion, Swimming III. International Series of Sports Sciences 8, pp. 70–109. Baltimore: University Park Press.

[24] Berger, M.A.M., Groot, G., Hollander, A.P., 1995. Hydrodynamic drag and lift forces on human hand arm models. Journal of Biomechanics, 28, 125–133.

[25] Clarys, J.P., 1979. Human morphology and hydrodynamics. In: J. Terauds and E. W. Bedingfield (Eds.), International Series on Sports Science 8; Swimming III, pp. 3–41, Baltimore, MD: University Park Press.

[26] Popa, C.V., Arfaoui A., Fohanno, S., Taïar, R., 2011 Polidori, G., 2014. Influence of a postural change of the swimmer's head in hydrodynamic performances using three dimensional CFD. Computer Methods in Biomechanics and Biomedical Engineering, 17(4), 344–351. CFD simulations of underwater swimming. Series in Biomechanics 24, 5–14.